Waves & Oscillations in the Solar Atmosphere:
Heating and Magneto-Seismology
Proceedings IAU Symposium No. 247, 2007
R. Erdélyi & C. A. Mendoza-Briceño, eds.

doi:10.1017/S1743921308015093

Twisting flux tubes as a cause of micro-flaring activity

D. B. Jess[1,2], R. T. J. McAteer[2], M. Mathioudakis[1], F. P. Keenan[1], A. Andic[1] and D. S. Bloomfield[3]

[1]Astrophysics Research Centre, School of Mathematics and Physics, Queen's University, Belfast, BT7 1NN, Northern Ireland, UK
email: djess01@qub.ac.uk

[2]NASA Goddard Space Flight Center, Solar Physics Laboratory, Code 671, Greenbelt, MD 20771, USA

[3]Max-Planck-Institut für Sonnensystemforschung, Max-Planck-Str. 2, 37191 Katlenburg-Lindau, Germany

Abstract. High-cadence optical observations of an H-α blue-wing bright point near solar AR NOAA 10794 are presented. The data were obtained with the Dunn Solar Telescope at the National Solar Observatory/Sacramento Peak using a newly developed camera system, the RAPID DUAL IMAGER. Wavelet analysis is undertaken to search for intensity-related oscillatory signatures, and periodicities ranging from 15 to 370 s are found with significance levels exceeding 95%. During two separate microflaring events, oscillation sites surrounding the bright point are observed to twist. We relate the twisting of the oscillation sites to the twisting of physical flux tubes, thus giving rise to reconnection phenomena. We derive an average twist velocity of 8.1 km/s and detect a peak in the emitted flux between twist angles of 180° and 230°.

Keywords. Sun: activity, Sun: atmospheric motions, Sun: evolution, Sun: flares, Sun: oscillations, Sun: photosphere

1. Introduction

Magnetic reconnection remains one of the most promising mechanisms to convert magnetic energy into heating of the local plasma (see Klimchuk 2006). Indeed, recent theoretical work by De Moortel & Galsgaard (2006a) suggests that photospheric footpoint motions lead to the build-up, and subsequent release, of magnetic energy. Recent work by Leenaarts *et al.* (2005) has discussed the formation of the H-α wing in detail using 3D magneto-convection simulations, and they show that H-α blue-wing bright points correspond to kiloGauss magnetic field concentrations in the photosphere. If reconnection processes are to be both temporally and spatially resolved, it is imperative to acquire data at the highest possible cadence using a sensitive camera system. Here we report intensity oscillations originating from an active region (AR) bright point, and the corresponding spatial rotation during microflare activity detected within the lower solar atmosphere.

2. Observations

The data presented here are part of an observing sequence obtained on 2005 August 10, with the Richard B. Dunn Solar Telescope (DST) at Sacramento Peak. Use of a highly sensitive, dual camera system enabled synchronized, simultaneous images at a rate of 20 frames per second in each camera to be obtained. Our optical setup allowed us to image a $50.4'' \times 49.2''$ region surrounding AR NOAA 10794 located at heliocentric co-ordinates ($770''$,$-254''$), or S12W56 in the solar NS-EW co-ordinate system. A Zeiss

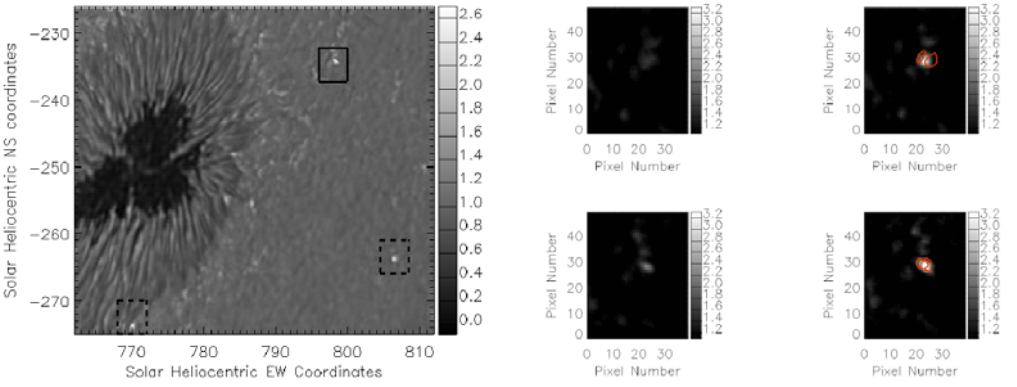

Figure 1. The left image shows the H-α blue wing field-of-view obtained at the DST in solar heliocentric coordinates. The colour scale indicates normalized flux and the solid box outlines the 40 × 50 pixel region removed for subsequent bright point analysis. The two dashed boxes outline additional bright points which were analysed for control purposes. The panel of four images on the right show the AR bright point before (upper left) and during (upper right) the first microflaring event. The lower left image displays the bright point prior to the second microflaring event, while the lower right image shows the bright point undergoing the second microflaring event. Overplotted in each diagram (red contours) are locations of strong oscillatory power at a periodicity of 20 s.

universal birefringent filter (UBF; Beckers *et al.* 1975) was used for H-α blue-wing (H-α core - 1.3Å) imaging with one of the RDI CCD detectors. In addition, a G-band filter was employed with the second RDI camera to enable synchronized imaging in the two wavelengths. Due to the smaller granulation contrast of H-α blue-wing images when compared to G-band data, only results obtained in the H-α blue wing are presented here. During the observational sequence used in the analysis, low-order adaptive optics was implemented.

The data selected for the present analysis consist of 31760 H-α blue-wing images taken with a 0.05 s cadence over a total time period of 26.5 min. These images have a spatial sampling of 0.1″ per pixel, to match the telescope's diffraction limited resolution in the H-α blue wing to that of the CCD. Further details regarding the RDI camera system can be found in Jess *et al.* (2007).

3. Data Analysis

Small-scale turbulent seeing in the Earth's atmosphere means that even high-order adaptive optics cannot compensate for all rapid air motions. Here we implement the speckle reconstruction masking method of Weigelt & Wirnitzer (1983), combining eighty raw RDI data frames for each speckle reconstruction, producing a new effective cadence of 4 s. Typical Fried parameters obtained prior to speckle reconstruction were $r_0 \approx 10$ cm, indicating good post-speckle image quality. Before commencing Fourier and wavelet techniques, a 40×50 pixel ($4'' \times 5''$) region surrounding the AR bright point under consideration (Fig. 1) was isolated for further study.

To compensate for camera jitter and large-scale air-pocket motions, all data was subjected to a Fourier co-aligning routine and de-stretched relative to simultaneous, high-contrast G-band images. After successful co-alignment and de-stretching, time series were created for each pixel before being passed into Fast Fourier Transform (FFT) and wavelet analysis routines. The Morlet wavelet was chosen for this study, and a number of strict cri-

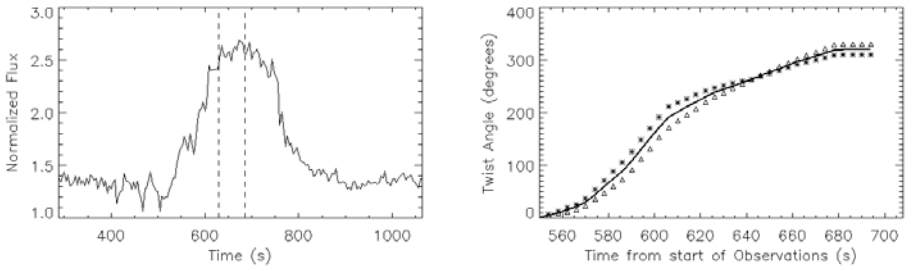

Figure 2. The left panel shows the AR bright point lightcurve where the intensity is computed by averaging pixel values which supersede a lower-intensity threshold of the background modal value plus 10σ. The vertical dashed line at 630 s corresponds to the time when the oscillatory power has undergone a 180° twist. The second vertical dashed line at 685 s corresponds to the time when the oscillatory power has undergone a 230° twist. The right panel shows the rotational angle of the footpoints as a function of time. The triangular and star symbols indicate the nature of the twisting for each of the oscillation sites, while the bold solid line shows the average rotational angle. As described in § 4, there is clearly an acceleration of the twist velocity between an angle of 20 and 160 degrees. Above 160 degrees, the twist velocity decelerates continually until the motion ceases.

teria implemented on the data allowed us to insure that oscillatory signatures correspond to real periodicities. These criteria have been described in detail in Banerjee *et al.* 2001.

Four-dimensional maps containing spatial information as well as wavelet power and oscillatory period were saved as outputs of wavelet analysis for detected oscillations which under the above criteria had a greater than 95% significance level. Furthermore, a time series was created for the AR bright point to display its temporal variability throughout the time sequence. Hence, variability in oscillatory phenomena can be compared readily with the bright point flux.

4. Results and Discussion

An examination of the bright point time series over the complete 26.5 min duration of the observations reveals two events which show intensity increases (Fig. 2). Due to the sharp rise in intensity and the corresponding decay pattern, we deem these intensity fluctuations to be characteristic of microflare activity with similar energetics and durations observed by Porter *et al.* (1987).

A succession of wavelet power diagrams around the time at which the microflaring activity occurs reveals a periodic signal. Prior to the commencement of both microflare events, there is an increase in oscillatory power superimposed, spatially, over the bright point (Fig. 1). The increase in oscillatory power provides two distinct regions of power separated by the central portion of the bright point. This increase in oscillatory power occurs 120 s prior to the second, larger microflare event which corresponds to 6 complete oscillation cycles for the 20 s periodicity plotted in Figure 1. During the evolution of both microflares, a spatial twist of the oscillatory sites occurs. The oscillation sites are not symmetric, yet appear to pivot around the bright point centre.

The path taken by the oscillating sites, after de-rotation to disk center, provides a perimeter distance of 17 pixels, corresponding to a traversed distance of 1230 km, while the duration of twisting is 148 s. The rotational movement of the oscillatory twist fails to complete a full 360° rotation, but we can use this distance to derive an upper limit to the average rotational velocity of the twisting oscillation sites, i.e. the twist velocity. Simply dividing the maximum traversed distance (1230 km) by the time taken (148 s), we

establish a maximum average twist velocity of ≈ 8 km/s, very close to the photopsheric sound speed (Fossum & Carlsson 2005). To demonstrate the temporal characteristics of the twist velocity, Figure 2 plots the rotational twist angle as a function of time. From this figure it is clear that the rotational motion is accelerated between twist angles of 20° and 160°, before being decelerated at rotational angles exceeding 160°.

Introducing the theoretical work by De Moortel & Galsgaard (2006a), we can interpret the oscillatory sites described above as a bundle of initially aligned, thin flux tubes. Even though we cannot directly see the flux tubes, material flowing along such paths may induce magneto-acoustic oscillations, which we can detect with the wavelet analysis applied to the data. The De Moortel & Galsgaard (2006b) model relates the evolution of the flux associated with magnetic reconnection to the rotational angle of initially aligned flux tubes.

Interpreting our results as having a non-zero background potential field (consistent with same-polarity flux domains), the peak reconnection rate should occur between a twist angle of 180° and 230°. Figure 2 shows the bright point time series during the second microflare event, along with vertical lines indicating the times where the twist angle equals 180° and 230°. From this plot it is clear there is a peak in the emissive flux between these two angles. Two other bright points in the same field of view were also analysed using the same criteria described in § 3. These bright points are of similar size and luminosity to the bright point in question (Fig. 1). We find no evidence for flaring in these two locations and there is no twisting of oscillatory power.

5. Concluding Remarks

We have presented direct evidence of high-frequency magneto-acoustic oscillations occurring in the immediate vicinity of an H-α blue-wing bright point. Periodicities as short as 15 s are found with significance levels greater than 95%. We have interpreted the rotational movement of oscillatory sites during microflare activity as the physical signature of flux tube twisting. We derive the rotational angle corresponding to maximum flux and the average twist velocity. This observational result is in qualitative agreement with the numerical model introduced recently by De Moortel & Galsgaard (2006a,b). A direct quantitative comparison with the model is not possible due to uncertainties associated with key input parameters such as resistivity, diffusivity, pressure, the distance between opposing line-tied plates and the corresponding degree of magnetic twist per unit length.

References

Banerjee, D., O'Shea, E., Doyle, J. G., & Goossens, M., 2001, *A&A*, 371, 1137

Beckers, J. M., Dickson, L., & Joyce, R. S., 1975, A Fully Tunable Lyot-Öhman Filter (AFCRL-TR-75-0090; Bedford: AFCRL)

De Moortel, I., & Galsgaard, K., 2006, *A&A*, 451, 1101

De Moortel, I., & Galsgaard, K., 2006, *A&A*, 459, 627

Fossum, A., & Carlsson, M., 2005, *Nature*, 435, 919

Jess, D. B., Andić, A., Mathioudakis, M., Bloomfield, D. S., & Keenan, F. P., 2007, *A&A*, 473, 943

Klimchuk, J. A., 2006, *Solar Phys.*, 234, 41

Leenaarts, J., Sütterlin, P., Rutten, R. J., Carlsson, M., & Uitenbroek, H., 2005, ESA-SP, 596

Porter, J. G., Moore, R. L., Reichmann, E. J., Engvold, O., Harvey, K. L., 1987, *ApJ*, 323, 380

Weigelt, G., & Wirnitzer, B., 1983, Optics Letters Vol. 8, No. 7, 389